JOURNAL OF THE KOREAN ASTRONOMICAL SOCIETY
36: S29 ~ S36, 2003

SOLAR ACTIVE REGION STUDY USING MICROWAVE MAPS

SU-CHAN BONG[1], JEONGWOO LEE[2], DALE E. GARY[2], AND HONG SIK YUN[1]
[1]Astronomy Program, SEES, Seoul National University, Seoul, 151-747, Korea
E-mail: scbong@astro.snu.ac.kr
[2]Department of Physics, New Jersey Institute of Technology, Newark, NJ 07102, USA

ABSTRACT

Quiescent solar radiation, at microwave spectral regime, is dominated by gyroresonant and thermal Bremsstrahlung radiations from hot electrons residing in solar active region corona. These radiations are known to provide excellent diagnostics on the coronal temperature, density, and magnetic field, provided that spatially resolved spectra are available from observations. In this paper we present an imaging spectroscopy implemented for a bipolar active region, AR 7912, using the multifrequency interferometric data from the Owens Valley Solar Array (OVSA), as processed with a new imaging technique, so-called Spatio-Spectral Maximum Entropy Method (SSMEM). From the microwave maps at 26 frequencies in the range of 1.2–12.4 GHz at both right- and left-circular polarizations, we construct spatially resolved brightness spectra in every reconstructed pixel of about 2 arcsec interval. These spectra allowed us to determine 2-D distribution of electron temperature, magnetic field of coronal base, and emission measure at the coronal base above the active region. We briefly compare the present result with existing studies of the coronal active regions.

Key words : Sun: corona—Sun: magnetic fields—Sun: radio radiation—sunspots

I. INTRODUCTION

Measurement of the physical parameters in the solar corona has been one of the major goals being pursued in solar physics, as is critical for many unsolved problems of solar physics. For instance, a relationship between the coronal temperature and magnetic fields is of interest to the coronal heating problem (Lee et al. 1998), and the coronal density and magnetic field provides the coronal Alfvén speed, a fundamental parameter in various magnetohydrodynamic processes in solar corona (Priest 1982). A difficulty in achieving this goal lies in that the corona is too tenuous to provide sufficient opacity to most of the radiations detectable on the ground. With recent space-borne solar instruments such as Yohkoh and SoHO, the goal of measuring coronal temperature and density is actively being pursued at EUV/UV or X-ray wavelengths (e.g., Nitta et al. 1991; Brosius et al. 1997; Zhang et al. 2001). On the other hand, microwave radiation has provided a ground-based means for observing the solar corona because the high electron temperature and magnetic field above active regions provide sufficient opacity at the microwave wavelengths. In this paper, we present our recent progress in the microwave study of a solar active region corona.

The property that makes microwave radiation sensitive to the coronal magnetic field is the fact that solar active regions of high magnetic field strength are generally optically thick due to gyroresonant opacity at frequencies above 3 GHz (Zheleznyakov 1962; Zlotnik 1968a, 1968b; White & Kundu 1997). Since this is the resonant property, the temperature and magnetic field measured from the observation pertains to a very thin region satisfying the gyroresonant condition. This is in contrast with other astronomical observations in which the observed quantity is always involved with the line-of-sight integration. When the coronal field is too weak to provide the gyroresonant opacity, there is always opacity due to thermal Bremsstrahlung which provides a diagnostic for emission measure of the electrons. It is important that this microwave radiation is involved with free electrons, and as a result, the microwave radiation provides clean measure of the plasma density and and magnetic field without complications arising from abundance of other elements.

The microwave radiation as a stand-alone diagnostic tool for solar active region has been addressed in various ways. The first approach was put forward by Hurford & Gary (1986) who proposed an idea that an observed dimension of microwave source represents the area filled with magnetic fields with strength greater than a critical field strength required for the gyroresonance opacity. Lee, Hurford, & Gary (1993) adopted this idea to convert successive change of microwave source size with frequency, as observed using the OVSA, to spatial distribution of magnetic field above a symmetric sunspot. Lee et al. (1997) utilized the same idea to further argue that comparison of the field strength inferred from observation with that predicted by a coronal field extrapolation can be used to test whether or not the coronal field is potential. The microwave tomography proposed by Aschwanden et al. (1995) also makes use of the gyroresonant property in such a way that the microwave source area observed at

Corresponding Author: S.-C. Bong

different viewing angles is related to a perspective view of the 3-D structure of the coronal magnetic field.

The second approach is microwave imaging spectroscopy. Gary & Hurford (1994) and Komm, Hurford, & Gary (1997) produced a set of spatially resolved brightness temperature spectra on a point-by-point basis from the multi-frequency interferometric data obtained with the OVSA. Such spectra constructed with sufficiently high spectral resolution allowed them to determine the dominant radiation mechanism, magnetic field, and plasma parameters solely based on the microwave observation. Gary & Hurford (1994) presented the resulting 2-D maps of coronal magnetic field and plasma parameters, the former of which is called a *coronal magnetogram.*

As the third approach, Lee et al. (1999) demonstrated a method to infer the 3-D coronal structure from high resolution microwave maps. The idea is based on the fact that in the solar corona, electric conductivity along a field line is much higher than across the field line, and therefore physical quantities pertaining to different layers of the corona, as represented by the multi-frequency maps, should show a good correlation at points connected via common field lines. Looking for such correlation in a given model of coronal field extrapolation leads to a test for the model, and thus information on the 3-D magnetic structure. Further comparison of the correlation between the microwave map with the photospheric magnetogram appears to provide a clue to the coronal heating problem too (Lee et al. 1998).

In most other observations, microwave imaging is made at a few frequencies, and independent diagnostics for coronal plasma parameters are needed to complement the above-mentioned microwave diagnostic on magnetic field (e.g. Strong et al. 1984; Webb et al. 1987). In particular, during the Coronal Magnetic Structures Observing Campaign (CoMStOC) a systematic study of the coronal magnetic field has been carried out using microwave maps obtained with the VLA and EUV/Soft X-ray maps from Yohkoh/SXT and SERT (Nitta et al. 1991; Schmelz et al. 1992, 1994; Brosius et al. 1992, 1997). In their approach, the plasma parameters are derived from the EUV and X-ray data, which are then used in the calculation of theoretical gyroresonance and thermal Bremsstrahlung opacity to help inferring the dominant radiation mechanism and the relevant harmonic. As a difference from the above-mentioned first and second approaches, this approach uses an observing frequency rather than the turn-over frequency, and the resulting diagnostic corresponds to some unknown coronal height.

An important result learned from the CoMStOC is that the temperature inferred from the microwave maps is found to be lower than the temperature from the soft X rays, leading to a speculation of cool materials lying over the hot materials above active regions (Schmelz et al. 1992, 1994). To some extent the discrepancy might be associated with the uncertainty in the abundance of the elements to which EUV/X-ray diagnostics are sensitive (Zhang et al. 2001). Similarly, Klimchuk & Gary (1995) compared microwave maps with soft X-ray map from Yohkoh/SXT and concluded that microwave emission and soft X-ray emission might represent different constituents of the solar atmosphere.

In this paper, we use microwave data for the study of the corona above a bipolar active region using the radio data obtained with the OVSA. Although we will employ the same technique implemented by Gary & Hurford (1994), we have a couple of motivations. First, we use an improved imaging reconstruction software designed for imaging spectroscopy in particular (Komm et al. 1997; S.-C. Bong, et al., in preparation), which will help complementing the sparse uv coverage of the array. Second, the target of the observation was a bipolar active region and the leading and trailing spots may show differing thermodynamic properties of interest. Our main goal in this paper is to determine the coronal parameters using solely the microwave data so that the results can then be compared with other data, i.e., soft X ray, as independent diagnostics.

II. OBSERVATION

The target was a solar active region, NOAA 7912, on 1995 October 11. According to the Hα filtergram and longitudinal magnetogram taken at Big Bear Solar Observatory (BBSO), the active region was located at S11, E59 near the southeastern limb, and consisted of a leading spot with stronger magnetic fields in the negative polarity and a trailing spot with weaker fields in the positive polarity. Soft X-ray maps from Yohkoh/SXT indicate that these two sunspots are connected to each other through a coronal loop, which is perhaps projected into the southeastern sky. The bright soft X-ray emission is more concentrated above the trailing spot, and it was of major interest in the current investigation how the microwave brightness distribution will be related to the soft X-ray structure.

(a) Data

At the time of this observation, the OVSA consisted of five antennas—two 27-m diameter dishes located at 61 and 488 m east, one 2-m dish at 183 m west and two 2-m dishes at 122 and 366 m north of the center of the array. These five antennas form 10 interferometer baselines, but only the seven baselines which include at least one of the two 27-m antennas were recorded and are available for this study. The array was operated with an observing sequence that sampled 45 frequencies in the range 1–18 GHz, in both right- and left-hand circular polarization (RCP and LCP respectively) every 12 s. The amplitudes and phases were calibrated with respect to our primary flux calibrator, 3C 84, which in turn was calibrated relative to the flux standard 3C 286. There was external interference at 1.0 GHz, and the active region showed no emission (above the noise

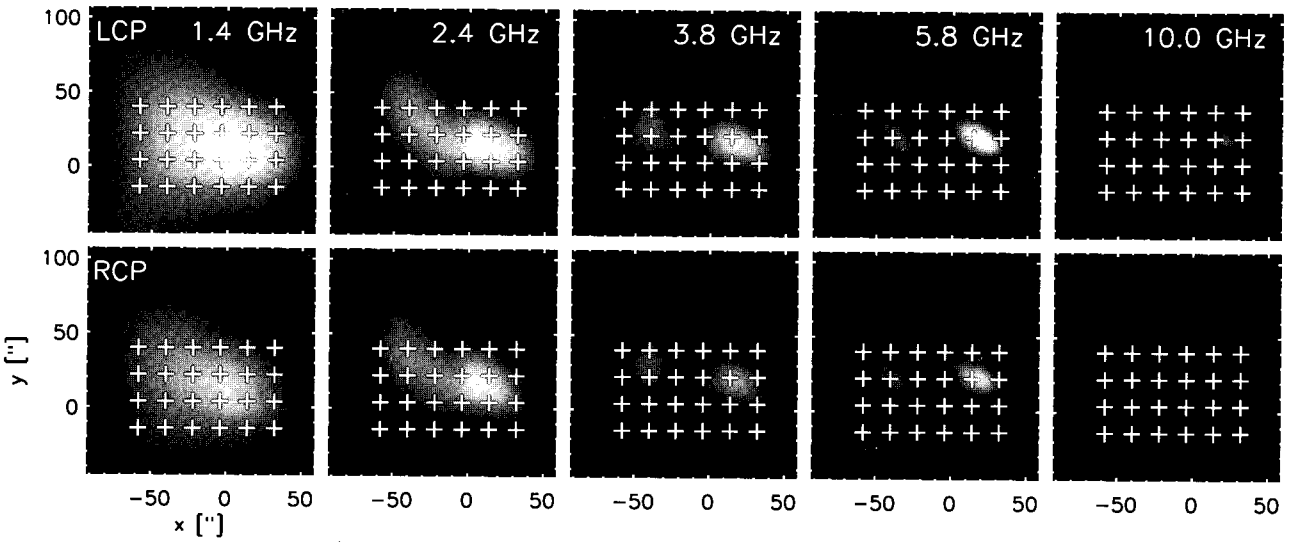

Fig. 1.— Reconstructed maps of AR 7912 in LCP (*upper row*) and RCP (*lower row*) for five selected frequencies. The gray scale in these maps ranges from 0 to 2.5 MK. Geographic north is up and east is to the left. The tick values in x, y axes are in arcsec from the center of the reconstructed image. The crosses (+) mark the locations selected for display of the spectra in Figure 2.

level) at the highest frequencies. Thus only the data of 26 frequencies in the range of 1.2–12.4 GHz, which showed relatively good quality, are used in this study. The observation time spanned the hours from 15:58 UT to 21:33 UT, and the flare occurred between 19:35 UT and 20:00 UT. To reconstruct radio images of the active region, we used data from 15:58 UT to 19:31 UT and from 20:22 UT to 21:33 UT to make rotational synthesis maps at each frequency. Solar rotation was taken into account by a phase correction.

Since the OVSA has a small number of baselines, the recorded visivilities cover the *uv* only sparsely, which produces sidelobes at a considerable level. Although the conventional reconstruction method such as CLEAN and Maximum Entropy Method (MEM) can reduce the sidelobes to some extent, an algorithm that utilizes the unusually large number of frequencies of the OVSA in imaging is considered more desirable. For this goal, Komm et al. (1997) developed so-called Spatio-Spectral Maximum Entropy Method (SSMEM) in which an entropy term associated with spectral distribution is introduced in addition to the conventional spatial entropy term, which as a whole leads to the smoothness in both spatial and spectral domain, as suitable for an imaging spectroscopy. Recently this technique has further been developed to allow 2-D spectral imaging together with refinement in algorithms of the entropy maximization and data constraint (S.-C. Bong, et al. in preparation). We applied the most up-to-date algorithm of the SSMEM to the OVSA data in order to implement the 2-D imaging spectroscopy.

(b) Microwave Maps

Figure 1 shows part of the reconstructed maps of AR 7912 in both polarizations at 5 selected frequencies. The reconstructed field of view was $295'' \times 295''$ at 10 GHz and inversely proportional to the frequency; the map center $(0'', 0'')$ in Figure 1 corresponds to $(-620'', -575'')$. The white crosses (+) in the maps indicate the location selected for display of the spectra in Figure 2.

The microwave emission appears in a single source at low frequencies (< 3 GHz) and changes to double sources at higher frequencies. For low frequencies up to 2.0 GHz, the maps show a broad single source covering the whole active region with maximum brightness temperatures up to 2.3 MK. The source is extended to the northeast and decreases in area with increasing frequency. We also notice the rather faint southeastern extension at lowest frequencies. This perhaps represents a large loop connecting the two spots, which we could also see in the soft X-ray images of Yohkoh (not shown in this paper). The maps from 2.0 GHz to 4.0 GHz show a transition from one broad source to two separate sources with the one associated with the leading spot and the other located near the trailing spot. These two sources are from now on referred to as the leading and the trailing sources. The brightness temperature is generally higher in LCP than in RCP, because emission from the leading spot in negative magnetic polarity is stronger.

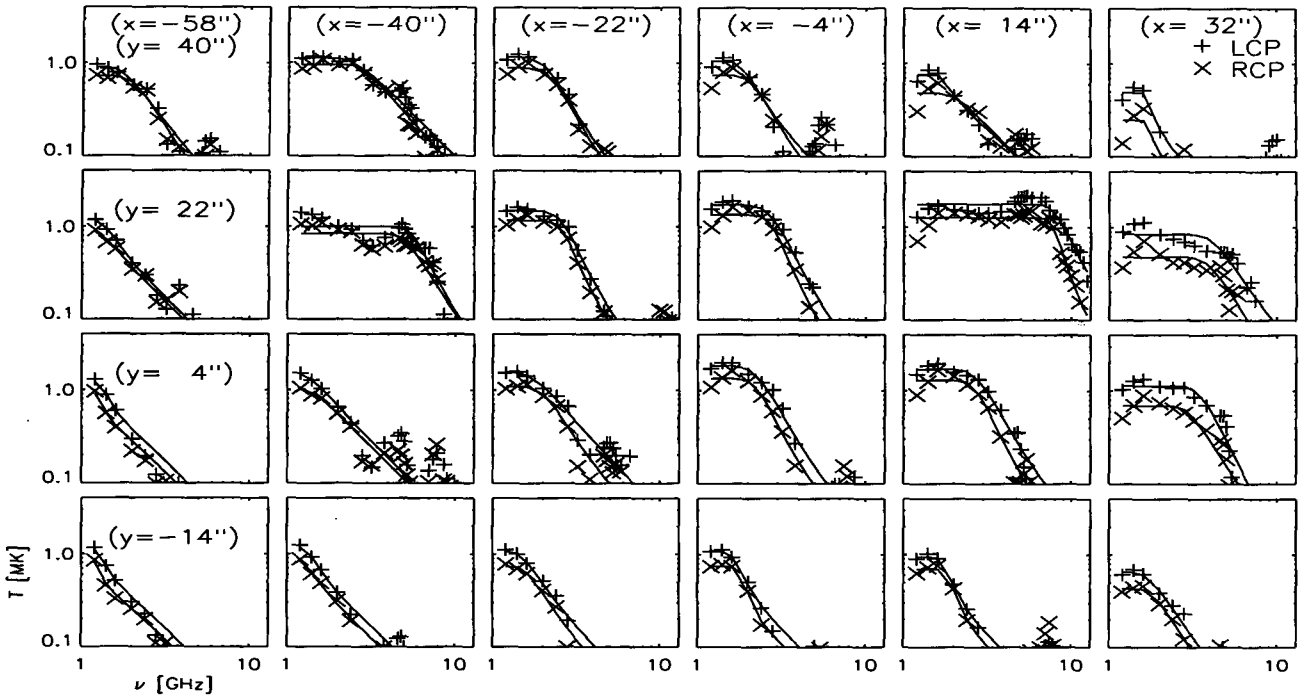

Fig. 2.— Reconstructed spectra at the selected locations as marked in Figure 1. Symbols are the observed spectra, and the solid lines represent model fitting to the observed spectra at each polarization. The upper (lower) curves are the fit to the LCP (RCP) spectra. The left panels are to the east and upper panels are to the north.

(c) Microwave Spectra

From the full set of 26 maps in two polarizations (52 maps in all), we can produce microwave spectra at any point by essentially stacking the maps into a data cube and taking a vertical cut at each point. We evaluated the brightness temperature maps on a 128×128 grid of $\sim 2''$ pixel (the pixel size in 12.4 GHz) and the values were interpolated from the reconstructed maps at lower frequencies. In Figure 2 we plot the spatially-resolved spectra at both polarizations with two different symbols. The solid lines represent fitting of the observed spectra (symbols) to our model spectrum to be discussed in the below (Eq. [3]). The panels in Figure 2 are arranged in such a way that each panel corresponds to the point marked by the crosses in Figure 1.

The spectrum at $(14'', 22'')$ in the second row and fifth column lies directly over the bright source at intermediate frequencies, and corresponds to emission from the leading sunspot in the region. The shape of this spectrum agrees well with that found directly over a sunspot in Gary & Hurford (1994) in that it shows the rising spectrum from 1.5 MK at 3 GHz to over 2 MK at 5 GHz indicating a hotter corona at lower heights. The spectrum at $(-40'', 22'')$ in the second row and second column overlies the weaker source at intermediate frequencies, and corresponds to emission associated with the trailing spots in the region. Spectra located between the leading and the trailing sources show rather flat spectrum up to 2 GHz, which rolls off at higher frequencies. At least some of those spectra, for example at $(-40'', 40'')$, and most of the southeastern spectra have a negative slope near -2 as expected for thermal Bremsstrahlung emission from coronal loops.

III. ANALYSIS

We now adopt the method of Gary & Hurford (1994) in order to derive the physical parameters from the spatially-resolved spectra shown in Figure 2. The idea is based on the approximate brightness temperature spectrum in the form:

$$T_b(x, y, \nu) \approx T_e(x, y)\left[1 - e^{-\tau(x,y,\nu)}\right] \qquad (1)$$

which can be approximated as $T_b \approx T_e$ at $\tau > 1$. In such spectrum, the radiation mechanism can be determined by looking at how rapidly the brightness temperature decreases with frequency at $\nu > \nu_{(\tau=1)}$ because

$$T_{b,\nu} \approx \tau_\nu T_e \propto \begin{cases} \nu^{-2} \\ \nu^{-q} \end{cases} \qquad (q > 5) \qquad (2)$$

for the case of thermal Bremsstrahlung and gyroresonant opacity is dominant, respectively.

In the present analysis, we use a composite opacity in (1), i.e. the opacity consists of gyroresonant and thermal Bremsstrahlung opacities, $\tau = \tau_f + \tau_g$, and

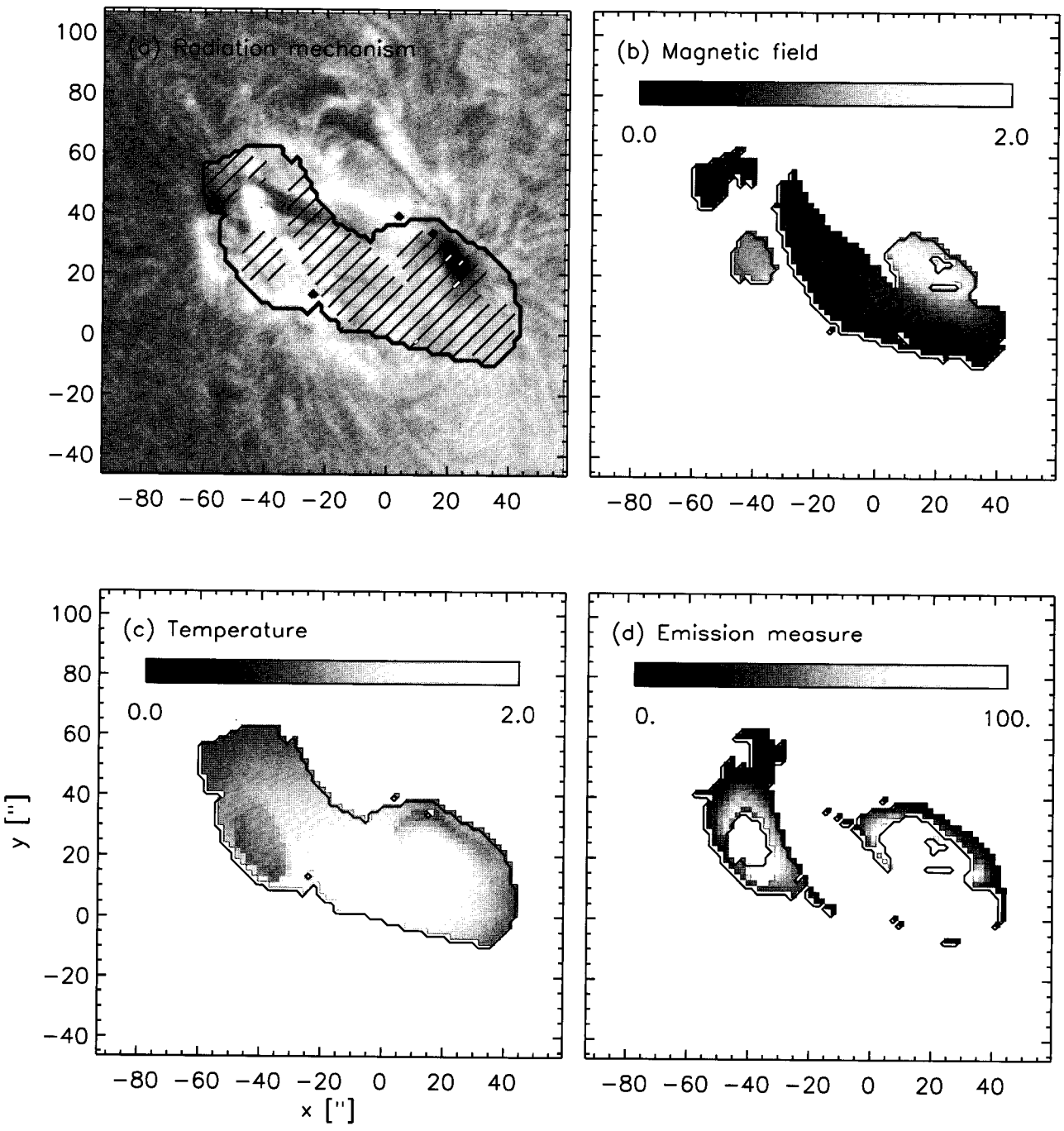

Fig. 3.— Maps of radiation mechanism, magnetic field strength, electron temperature, and emission measure in the coronal part of the active region, NOAA 7912, as derived from the spatially-resolved spectra. (*a*) The thick contour outlines the optically thick region and the oblique lines mark the regions where gyroresonant emission dominates. The background image is Hα filtergram taken at BBSO at 22:29:44 UT on 1995 Oct 11. (*b*) The magnetic field is shown as grey scale in units of kG in regions where the gyroresonant emission dominates. (*c*) Electron temperature in units of MK. (*d*) Electron emission measure is shown in units of $10^{27}\mathrm{cm}^{-5}$ in regions where the free-free emission dominates.

assume that these opacities can be represented by some basic spectral forms such as:

$$\tau_f = \left(\frac{\nu}{\nu_f}\right)^{-2} \quad \text{and} \quad \tau_g = \left(\frac{\nu}{\nu_g}\right)^{-q} \qquad (q > 5) \quad (3)$$

where ν_g and ν_f are the transition frequency for the gyroresonat and thermal Bremsstrahlung opacities, respectively. Thus we take (T_e, ν_g, ν_f, q) as free parameters which are adjusted to fit the observed spectrum as closely as possible. We note here that τ_g is not real optical depth of the gyrosonance emission, but is adopted just to make the rapidly decreasing spectrum. Examples of this fitting are shown in Figure 2 as solid lines. From the resulting model parameters (T_e, ν_g, ν_f, q), we derive the dominant radiation mechanism, coronal electron temperature, magnetic field, and the column emission measure. The results are shown in Figure 3 and are described in the below.

(a) Radiation Mechanism

For our model fitting, the observed spectrum should contain the optically thick part in low frequencies to determine T_e, and also the optically thin part to allow determination of the spectral slope q. We arbitrarily defined the optically thick region as where the higher transition frequency is greater than 2 GHz and $T_e > 0.7$ MK. And the gyroresonance dominant region as $\tau_g > \tau_f$ when $\tau_f = 0.2$. The result map of radiation mechanism is shown in Figure 3(a), in such a way that the thick contour encloses the optically thick region and slanted lines cover the gyroresonance dominant part. The result shows that the gyroresonant regions are located above the leading spot, while the thermal Bremsstrahlung emission is mostly from the trailing spot. It appears that the former is associated with stronger field strength above the leading spot and the latter is with the higher density in the trailing spot. The region dominated by the thermal Bremsstrahlung emission coincides with the region of brighter soft X-ray emission. Relatively small region near and between the spots were optically-thick and the gyroresonance emission is dominant in most of that region. However, thermal Bremsstrahlung emission was more widely spread around the trailing spot than the leading spot.

(b) Magnetic Field

The gyro-resonance emission is due to resonance between the electron gyro-motion and the microwave. This resonance occurs only within thin resonance layers which match the resonance condition $\nu \approx s\nu_B$. Here ν is the observing frequency, $\nu_B \approx 2.8 \times 10^6 B$ is the electron gyro-frequency, and s is a small integer harmonic number. At grid points where thermal gyroresonance is the dominant emission mechanism we calculate the maximum magnetic field strength in the corona, B_{max} as follows (e.g. White & Kundu 1997):

$$B_{max} = \frac{\nu_g}{2.8 \times 10^6 s}, \qquad (4)$$

where the harmonic number, s, is either 2 or 3 and $\nu_g = \nu_{(\tau_g=1)}$. Since ν_g is continuous with spatial position in the gyroresonance dominant region, we assume $s = 3$ at all grid points (cf. Lee, Hurford, & Gary 1993; Gary & Hurford 1994).

Figure 3(b) shows a map of B_{max} in grayscale ranging from 0.0 to 2.0 kG. The derived magnetic field is drawn only in the region where the spectrum is found to be of gyroresonant emission. As a result the leading spot shows the strongest magnetic field strength reaching ~1700 G, while the trailing source has maximum field strength of ~1300 G in the corona. The height of these coronal magnetic field lies in 2–5 Mm above the photosphere.

(c) Plasma Parameters

The electron temperature can be determined for all regions where the relatively flat part of brightness temperature is found, independent of radiation mechanism. Figure 3(c) shows the electron temperature in grayscale image ranging from 0.0 to 2.0 MK for the same area covered in Figure 3(a). The highest electron temperature reaches ~2.0 MK found at the southeast of the leading spot. This could be the result of the projection effect where the hot electrons in the coronal loop above the leading spot is projected toward the limb. A relatively cooler region is found around the leading sunspot which outlines the enhanced temperature in the spectrum discussed earlier in §II(c). Since the enhancement has high temperature in the inner part, and low temperature in the outer part of the region, the overall flat part of the fitted spectrum is lowered and the apparent cool region results. Because this enhancement of temperature up to 2.4 MK does not extend to lower frequencies, we presume that it must lie below the $T_e \sim 2$ MK coronal loop.

The electron emission measure or density can be determined in regions where thermal Bremsstrahlung is found to dominate the emission. We calculate the column emission measure as follows (e.g. Dulk 1985):

$$\int n_e^2 dl \approx 4.8 \nu_f^2 \, T_e^{3/2} \mathrm{cm}^{-5}. \qquad (5)$$

Figure 3(d) shows a map of the column emission measure in the region where the spectrum is not gyroresonance type. The greyscale ranges from 0 to $100 \times 10^{27} \mathrm{cm}^{-5}$. As shown in Figure 3($a$), most of the optically thick region shows gyroresonant spectrum, except some areas with high electron density and low magnetic field. The thermal Bremsstrahlung spectrum is found in the areas widely spread around the trailing spot, reflecting the weaker magnetic field there. We also found that the emission measure is greater near the spots.

IV. SUMMARY

In this paper, we have presented a microwave imaging spectroscopy implemented for a bipolar active region AR 7912 with the OVSA data. For imaging, we have combined rotational synthesis with so-called SSMEM reconstruction technique to complement the sparse *uv* coverage of the array. Although observations with better spatial resolution and better image quality are needed to avoid some of the ambiguities that remain, the SSMEM algorithm has helped in this regard and form an important part of our understanding of the structure and activity of the solar corona.

We have applied Gary & Hurford's (1994) procedure to determine the present data set in order to determine the dominant radiation mechanism, magnetic field, and plasma parameters above the active region on a point-by-point basis. Our results are summarized as follows.

1. By studying the spatially resolved brightness temperature spectra, derived from the multifrequency images on a nearly 2″ grid over the entire active region, we confirm that large part of the emission associated with the active region is thermal gyroresonance emission, while outskirt of the emission of the trailing spot is dominated by thermal Bremsstrahlung (cf. Gary & Hurford 1987).

2. We found that the magnetic field strength in this active region is > 160 G over the most of the active region. The leading spot has higher coronal field strength exceeding 1000 G over most of the region, reaching a maximum of 1700 G.

3. The electron temperature, T_e, is less than 2×10^6 K in all part of the active region. The brightness temperature maximum of $> 2 \times 10^6$ K near 5.4 GHz is localized at the trailing edge of the leading sunspot. This may indicate a volume of hot material located beneath cooler ($< 2 \times 10^6$ K) coronal material, similar to the case found in the studies by Gary & Hurford (1994) and Aschwanden et al. (1995).

4. The column emission measure is found in the range of $\sim$(6–100) $\times 10^{27}$ cm^{-5} in the regions with thermal Bremsstrahlung emission. This yields a volume emission measure of $\sim(0.9\text{–}3.8)\times 10^9$ cm^{-3}, assuming a typical coronal scale height of $0.1R_\odot = 7 \times 10^9$ cm.

The stronger leading spot was dominated by the gyroresonance spectrum. Since the leading spot has stronger magnetic field, the emission is therefore from the resonance layer lying at relatively high corona, making the thermal Bremsstrahlung above the resonance layer very weak. On the other hand the following spot has weaker coronal field in the corona and gyroresonance layer locates low and the passage along the line of sight could gather the thermal Bremsstrahlung opacity more probably.

Further comparison with the Yohkoh/SXT data for this active region indicates that the soft X-ray emission is brighter in the trailing sunspot whereas microwave emission is brighter in the leading spot. This result qualitatively agrees to the well-known fact that microwave and soft X-ray brightness are not well correlated with each other and the soft X-ray emission is depressed above sunspots. However, our results that the microwave emission is stronger at the leading sunspot with stronger magnetic field does not agrees to the conventional result that sunspots always contain the lowest temperatures and emission measures in the active regions (see, for instance, Nindos et al. 2000). These inconsistent results should be further investigated in future. However, it could simply be due to the fact that the present study used all range of frequencies including optically thick frequencies whereas the previous investigations using the Nobeyama Heliograph rely on 17 GHz only which tends to be optically-thin in most cases.

In addition, we note that the concentration of hot material ($> 2 \times 10^6$ K) low in the trailing edge of the leading sunspot may be a phenomenon similar to the cool material lying amid hot material found during the CoMStOC (Schmelz et al. 1992; Brosius et al. 1992). On general ground we can regard this as evidence for inhomogeneous structure of coronal temperature.

Our main goal in this paper has been kept to the demonstration of microwave imaging spectroscopy as a utility to determine 2-D distribution of the coronal magnetic field and plasma parameters. It however appears to be of new interest whether the diverse distribution of electron temperature and magnetic field found in this bipolar active region will have an implication on the recent coronal heating modelling (e.g., Y. Mok, et al. in preparation). Such comparison of the present result with the soft X ray data and the theoretical model for solar active regions will be presented in a companion paper.

ACKNOWLEDGEMENTS

This work was financially supported by the BK21 Project of the Korean Government. JL has been supported by NASA grants NAG 5-10891 and NAG-11875. The OVSA is supported by NSF grant AST-9987366 to NJIT. S.-C. Bong would like to express his sincere thanks to Professor Yun who has kindly supervised him.

REFERENCES

Aschwanden, M. J., Lim, J., Gary, D. E., & Klimchuk, J. A. 1995, Solar Rotation Stereoscopy in Microwaves, ApJ, 454, 512

Brosius, J. W., Willson, R. F., Holman, G. D., & Schmelz, J. T. 1992, Coronal Magnetic Structures Observing Campaign. IV - Multiwaveband Observations of Sunspot and Plage-associated Coronal Emission, ApJ, 386, 347

Brosius, J. W., Davila, J. M., Thomas, R. J., & White, S. M. 1997, Coronal Magnetography of a Solar Active Region Using Coordinated SERTS and VLA Observations, ApJ, 488, 488

Dulk, G. A. 1985, Radio Emission from the Sun and Stars, ARA&A, 23, 169

Gary, D. E., & Hurford, G. J. 1987, Multifrequency Observations of a Solar Active Region during a Partial Eclipse, ApJ, 317, 522

Gary, D. E., & Hurford, G. J. 1994, Coronal Temperature, Density, and Magnetic Field Maps of a Solar Active Region Using the Owens Valley Solar Array, ApJ, 420, 903

Hurford, G. J., & Gary, D. E. 1986, Measurement of Coronal Fields Using Spatially Resolved Microwave Spectroscopy, in NASA Conf. Proc. 2442, Coronal and Prominence Plasmas, ed. A. I. Poland (Washington: NASA), 319

Klimchuk, J. A., & Gary, D. E. 1995, A Comparison of Active Region Temperatures and Emission Measures Observed in Soft X-Rays and Microwaves and Implications for Coronal Heating, ApJ, 448, 925

Komm, R. W., Hurford, G. J., & Gary, D. E. 1997, A Spatial and Spectral Maximum Entropy Method as Applied to OVRO Solar Data, A&AS, 122, 181

Lee, J., Hurford, G. J., & Gary, D. E. 1993, Microwave Emission from a Sunspot. I - Implications for the Sunspot Magnetic Structure, Sol. Phys., 144, 45

Lee, J., White, S. M., Gopalswamy, N., & Kundu, M. R. 1997, Signatures of Coronal Currents in Microwave Images, Sol. Phys., 174, 175

Lee, J., McClymont, A. N., Mikić, Z., White, S. M., & Kundu, M. R. 1998, Coronal Currents, Magnetic Fields, and Heating in a Solar Active Region, ApJ, 501, 853

Lee, J., White, S. M., Kundu, M. R., Mikić, Z., & McClymont, A. N. 1999, A Test for Coronal Magnetic Field Extrapolations, ApJ, 510, 413

Nindos, A., Kundu, M. R., White, S. M., Shibasaki, K., & Gopalswamy, N. 2000, Soft X-Ray and Gyroresonance Emission above Sunspots, ApJS, 130, 485

Nitta, N., et al. 1991, Coronal Magnetic Structures Observing Campaign. I - Simultaneous Microwave and Soft X-ray Observations of Active Regions at the Solar Limb, ApJ, 374, 374

Priest, E. R. 1982, Solar Magneto-hydrodynamics (Dordrecht: D. Reidel)

Schmelz, J. T., Holman, G. D., Brosius, J. W., & Gonzalez, R. D. 1992, Coronal Magnetic Structures Observing Campaign. II. Magnetic and Plasma Properties of a Solar Active Region, ApJ, 399, 733

Schmelz, J. T., Holman, G. D., Brosius, J. W., & Willson, R. F. 1994, Coronal Magnetic Structures Observing Campaign. 3: Coronal Plasma and Magnetic Field Diagnostics Derived From Multiwaveband Active Region Observations, ApJ, 434, 786

Strong, K. T., Alissandrakis, C. E., & Kundu, M. R. 1984, Interpretations of Microwave Active Region Structures Using SMM Soft X-ray Observations, ApJ, 277, 865

Webb, D. F., Holman, G. D., Davis, J. M., Kundu, M. R., & Shevgaonkar, R. K. 1987, The Plasma and Magnetic Field Properties of Coronal Loops Observed at High Spatial Resolution, ApJ, 315, 716

White, S. M., & Kundu, M. R. 1997, Radio Observations of Gyroresonance Emission from Coronal Magnetic Fields, Sol. Phys., 174, 31

Zhang, J., Kundu, M. R., White, S. M., Dere, K. P., & Newmark, J. S. 2001, Reconciling Extreme-Ultraviolet and Radio Observations of the Sun's Corona, ApJ, 561, 396

Zheleznyakov, V. V. 1962, The Origin of the Slowly Varying Component of Solar Radio Emission, Soviet Astron., 6, 3

Zlotnik, E. Ya. 1968a, Theory of the Slowly Changing Component of Solar Radio Emission. I., Soviet Astron., 12, 245

Zlotnik, E. Ya. 1968b, The Theory of the Slowly Changing Component of Solar Radio Emission. II., Soviet Astron., 12, 464